Journal of Zhejiang University-SCIENCE A (Applied Physics & Engineering)
ISSN 1673-565X (Print); ISSN 1862-1775 (Online)
www.jzus.zju.edu.cn; www.springerlink.com
E-mail: jzus@zju.edu.cn

Active control experiments on a herringbone ribbed cable dome*

Xiao-tian LIANG, Xing-fei YUAN†‡, Shi-lin DONG

Space Structures Research Center, Zhejiang University, Hangzhou 310058, China

†E-mail: yuanxf@zju.edu.cn

Received Apr. 26, 2017; Revision accepted Dec. 3, 2017; Crosschecked Aug. 7, 2018

Abstract: Active control experiments on a newly proposed herringbone ribbed cable dome are described in this study. The cables of the dome are designed to have the ability to change length in order to adjust the geometrical configuration and the force distribution of the structure. Thereby, the dome is adaptable to different load cases. To begin with, for achieving the control amount for the active control test, an active control algorithm based on a nonlinear force method is presented. Then, an assembly and pre-stressing procedure is implemented. Active adjustment tests on three possible types of adjustable cables are performed to provide a practical method for the following active control test. The active control test demonstrates the applicability of the active control algorithm to achieve both force control and shape control. The method can be used to prevent failure of the cable domes due to slackening of the ridge cables and excessive displacements of the central section of the cable dome. The experiments verify the proposed control algorithm and the feasibility of the cable dome to adapt to excessive full span load and maintain the integrity of the structure.

Key words: Herringbone ribbed cable dome; Active control; Nonlinear force method; Force control; Shape control
https://doi.org/10.1631/jzus.A1700228 **CLC number:** TU394

1 Introduction

The cable dome was proposed and established in Seoul, Korea by Geiger et al. (1986) who were inspired by Fuller (1962)'s idea of tensegrity. Tensegrity is the conjunction of the two words tension and integrity. Thanks to its light weight and high efficiency, the cable dome is extensively employed in large-span space structures around the world, such as the Georgia Dome in Atlanta (Levy, 1994), the Redbird Arena in Bloomington-Normal, the Amagi Dome in Japan, and the Taoyuan Arena in Taiwan, China. Despite their different shapes, all these cable domes comply with the rule that "the structure will have the aspect of continuous tension throughout and that the compression will be subjugated so that the compression elements become small islands in a sea of tension" (Fuller, 1962). Both ends of the struts in a cable dome are connected with cables, which ensures that all struts are isolated from each other. This study describes the active control experiments on a new form of cable dome, namely the herringbone ribbed cable dome, proposed by Dong and Liang (2014). The notable difference between the new dome and traditional cable domes is that the vertical struts are replaced by two herringbone struts. Horizontal projections of the struts become closed curves instead of the isolated nodes generated by a traditional cable dome.

Hitherto, most research has focused on the force and form finding (Wang et al., 2010; Li and Huang, 2011; Xi et al., 2011; Guo and Zhu, 2016), static behavior (Yuan and Dong, 2002; Li and Huang, 2011), dynamic behavior (Chen and Dong, 2011; Zhang et al., 2014; Wei et al., 2015), stability and failure analysis (Zhu et al., 2013; Kim and Sin, 2014)

‡ Corresponding author
* Project supported by the Zhejiang Provincial Natural Science Foundation of China (No. LZ14E080001) and the National Natural Science Foundation of China (Nos. 51278461 and 51578492)
ORCID: Xing-fei YUAN, https://orcid.org/0000-0003-0507-5039

of different cable domes. Generally, three types of failure occur in cable domes: structural instability caused by buckling of compressed struts, structural instability due to cable slackening, and structural failure due to rupture of the cables. Tang and Shen (1998) suggested that the cable dome would fail when the ridge cables became slack, whereas Zhu et al. (2013) proposed that the structure would retain its load-carrying capacity even after the slackening of the ridge cables. However, as the slackening of cables would cause a significant increase in nodal displacement and thus the folding or tearing of the membranes, a well-designed cable dome should be designed to prevent it.

With the emerging conception of active structures which have the ability to change the response of the structure to its environment (Soong and Manolis, 1987), an efficient method for traditional static and passive structures in civil engineering is available to help improve their ability to adapt to new challenges in extreme environments. Structural shape control can be achieved by changing the length of active members to improve the adaptability of structures under different environmental conditions.

As the implementation of fine tuning and adjustment is easier for tensegrity structures than conventional structures (Skelton and de Oliveira, 2009), tensegrity structures are commonly chosen as the subjects of active control research. The emergence of active control in tensegrity structures can be traced to the mid-1990s. Since that time, structures with high-precision control characteristics have gained the attention of many researchers (Oppenheim and Williams, 1997; Djouadi et al., 1998; van de Wijdeven and de Jager, 2005). A series of detailed studies was performed by the Swiss Federal Institute of Technology (EPFL). Two full-scale prototypes of tensegrity structures with three modules and five modules were constructed in the EPFL. The design, assembly, and static testing of the tensegrity structures, and the development of a stochastic search algorithm for shape control have been conducted in the laboratory (Fest et al., 2003, 2004). Later, Adam and Smith (2007) extended the concept of an adaptive tensegrity structure to self-diagnosis and to self-repair. A shape control framework which consisted of multi-objective search and reinforcement learning was experimentally validated on an active tensegrity structure (Adam and Smith, 2008). To assess the practicability of an active tensegrity structure in practice, Korkmaz et al. (2012) investigated the active control performance of a tensegrity bridge. Optimally directed locations of active cables were determined, and a multi-objective self-repair procedure was proposed to ensure the tolerance of the bridge to damage.

Unlike tensegrity structures which are self-equilibrated, cable domes require external ring beams to provide tension to support the whole structure. Different mechanical characteristics, configurations, and purposes of the application require different control approaches. A few numerical and experimental studies have been conducted to implement active control procedures for cable domes. Most research has used small-size laboratory prototypes that cannot reproduce the complex behavior of full-scale highly coupled structural systems. Kmet and Mojdis (2015) developed a Levy-form adaptive cable dome by adding a hydraulic actuator as the central compressed strut. The object of the experiment was to verify the adaptability of the cable dome to variable load cases by changing the length of the central strut.

This study develops an adaptive herringbone ribbed cable dome model to confirm the possibility of introducing variable length cables to improve the reliability of the structure. The aim is to find a new way to improve the carrying capacity of the cable dome. Thus, active control experiments are conducted to validate the practicability of the proposed method. To obtain the control amount for conducting the active control procedure, a nonlinear control method based on a force method is illustrated first. Next, the description of the dome is presented and the pre-stressing procedure of the cable dome is illustrated. Then, for determining which active members should be applied to the active control procedure, the active adjustment test is demonstrated. Furthermore, internal force control and nodal displacement control are actualized in an active control experiment to verify the proposed algorithm and to validate the applicability of the active control method to herringbone ribbed cable domes. Finally, discussion and suggestions for future studies are outlined in the conclusion.

2 Active control algorithm based on force method

With a clear notion of the mechanics and the strength to determine the modes of inextensional mechanisms and their states of self-stress, the force method is frequently applied to the analysis of indeterminate structures (Pellegrino and Calladine, 1986; Pellegrino, 1990; Pellegrino et al., 1992). The possibility of applying a linear force method to active control of the structure has been proven by You (1997). To improve the accuracy of the force method, Luo and Lu (2006) proposed a geometrically nonlinear force method by solving the nonlinear algebraic equations using an iteration procedure. Xu and Luo (2009) applied this method to prestressed cable structures without external force, to control selected nodal displacement. The concise expressions for force control and shape control are derived using pseudoinverse in this study. The procedure for obtaining the control amount is demonstrated in the following paragraphs.

The basic equations of the nonlinear force method when considering the geometrical nonlinear characteristics can be expressed as

$$\boldsymbol{A}^{(k)}(\boldsymbol{d})\delta\boldsymbol{t}^{(k)}=\delta\boldsymbol{f}^{(k)}, \tag{1}$$

$$\boldsymbol{B}^{(k)}(\boldsymbol{d})\delta\boldsymbol{d}^{(k)}=\delta\boldsymbol{e}^{(k)}, \tag{2}$$

$$\delta\boldsymbol{e}^{(k)}=\boldsymbol{F}^{(k)}(\boldsymbol{d})\delta\boldsymbol{t}^{(k)}, \tag{3}$$

where $\boldsymbol{A}$, $\boldsymbol{B}$, and $\boldsymbol{F}$ are the equilibrium matrix, the compatibility matrix, and the flexibility matrix, respectively. The vectors $\boldsymbol{f}$, $\boldsymbol{d}$, $\boldsymbol{t}$, and $\boldsymbol{e}$ denote the nodal loads, nodal displacements, axial force, and elongations in the members, respectively. The superscript k denotes that the formulae are built on step k. To analyze the equilibrium matrix, a singular value decomposition method is applied. Then $\boldsymbol{A}$ can be written as

$$\boldsymbol{A}=\boldsymbol{U}\boldsymbol{S}\boldsymbol{V}^{\mathrm{T}}=\begin{bmatrix}\boldsymbol{U}_{\mathrm{r}} & \boldsymbol{U}_{\mathrm{m}}\end{bmatrix}\begin{bmatrix}\boldsymbol{S}_{\mathrm{r}} & 0\\ 0 & 0\end{bmatrix}\begin{bmatrix}\boldsymbol{V}_{\mathrm{r}} & \boldsymbol{V}_{\mathrm{s}}\end{bmatrix}^{\mathrm{T}}, \tag{4}$$

where $\boldsymbol{U}_{\mathrm{m}}$ is the matrix of inextensional mechanisms and $\boldsymbol{U}_{\mathrm{r}}$ is the matrix of the left vectors of $\boldsymbol{U}$. $\boldsymbol{V}_{\mathrm{s}}$ is the matrix of states of self-stress and $\boldsymbol{V}_{\mathrm{r}}$ is the matrix of the left vectors of $\boldsymbol{V}$. $\boldsymbol{S}$ is the diagonal matrix and $\boldsymbol{S}_{\mathrm{r}}$ is the diagonal matrix of singular value. Then, the force solution of Eq. (1) can be expressed as the combination of the particular solution and the general solution:

$$\delta\boldsymbol{t}=(\boldsymbol{V}_{\mathrm{r}}\boldsymbol{S}_{\mathrm{r}}^{-1}\boldsymbol{U}_{\mathrm{r}}^{\mathrm{T}})\delta\boldsymbol{f}+\boldsymbol{V}_{\mathrm{s}}\boldsymbol{\alpha}, \tag{5}$$

where $\boldsymbol{\alpha}$ is a vector of the general solution. The expression of $\boldsymbol{\alpha}$ can be determined through the principle of virtual work.

Two procedures are conducted in the active control test: the loading process and the active control process. In the loading process, the coefficient vector $\boldsymbol{\alpha}$ has the following form:

$$\boldsymbol{\alpha}=-(\boldsymbol{V}_{\mathrm{s}}^{\mathrm{T}}\boldsymbol{F}\boldsymbol{V}_{\mathrm{s}})^{-1}(\boldsymbol{V}_{\mathrm{s}}^{\mathrm{T}}\boldsymbol{F}\boldsymbol{V}_{\mathrm{r}}\boldsymbol{S}_{\mathrm{r}}^{-1}\boldsymbol{U}_{\mathrm{r}}^{\mathrm{T}}\delta\boldsymbol{f}). \tag{6}$$

For the structure that has the proper pre-stress to restrain inextensional displacements, Eq. (2) can be expressed as

$$\delta\boldsymbol{d}=\boldsymbol{B}^{+}\delta\boldsymbol{e}, \tag{7}$$

where $\boldsymbol{B}^{+}$ is the Moore-Penrose pseudoinverse of $\boldsymbol{B}$.

The geometric nonlinear analysis can then be achieved by an iteration procedure. A detailed procedure for structural analysis is provided by Luo and Lu (2006).

In the active control procedure, $\delta\boldsymbol{f}$ is zero because the load is constant. Thus, the internal force increment has a linear relationship with the states of self-stress. The coefficient vector with the constant load in the active control procedure can be rewritten as

$$\boldsymbol{\alpha}=-(\boldsymbol{V}_{\mathrm{s}}^{\mathrm{T}}\boldsymbol{F}\boldsymbol{V}_{\mathrm{s}})^{-1}\boldsymbol{V}_{\mathrm{s}}^{\mathrm{T}}\delta\boldsymbol{e}_{\mathrm{s}}, \tag{8}$$

where $\boldsymbol{e}_{\mathrm{s}}$ is the vector of length variation in active members. $(\ )_{\mathrm{s}}$ indicates the vector in the control process. The relationship between the internal force and the control amount is given as

$$\delta\boldsymbol{t}_{\mathrm{s}}=-\boldsymbol{V}_{\mathrm{s}}(\boldsymbol{V}_{\mathrm{s}}^{\mathrm{T}}\boldsymbol{F}\boldsymbol{V}_{\mathrm{s}})^{-1}\boldsymbol{V}_{\mathrm{s}}^{\mathrm{T}}\delta\boldsymbol{e}_{\mathrm{s}}. \tag{9}$$

The elongation of the members in the active control process is caused by two factors, the active control

amount and the internal force. Then, the expression of the elongation of the members in the active control process can be written as

$$\delta \boldsymbol{e}_{\mathrm{s}}' = \delta \boldsymbol{e}_{\mathrm{s}} + \boldsymbol{F}\delta \boldsymbol{t}_{\mathrm{s}}. \tag{10}$$

Substituting Eq. (9) into Eq. (10), $\delta \boldsymbol{e}_{\mathrm{s}}'$ has the value:

$$\delta \boldsymbol{e}_{\mathrm{s}}' = \left[\boldsymbol{I} - \boldsymbol{F}\boldsymbol{V}_{\mathrm{s}}(\boldsymbol{V}_{\mathrm{s}}^{\mathrm{T}}\boldsymbol{F}\boldsymbol{V}_{\mathrm{s}})^{-1}\boldsymbol{V}_{\mathrm{s}}^{\mathrm{T}}\right]\delta \boldsymbol{e}_{\mathrm{s}}, \tag{11}$$

where $\boldsymbol{I}$ is the identity matrix. Then, the displacement increment is

$$\delta \boldsymbol{d}_{\mathrm{s}} = \boldsymbol{B}^{+}\left[\boldsymbol{I} - \boldsymbol{F}\boldsymbol{V}_{\mathrm{s}}(\boldsymbol{V}_{\mathrm{s}}^{\mathrm{T}}\boldsymbol{F}\boldsymbol{V}_{\mathrm{s}})^{-1}\boldsymbol{V}_{\mathrm{s}}^{\mathrm{T}}\right]\delta \boldsymbol{e}_{\mathrm{s}}. \tag{12}$$

After obtaining Eqs. (9) and (12), the force and shape control can be achieved based on these two equations. For simplicity, Eqs. (9) and (12) can be rewritten as

$$\delta \boldsymbol{t}_{\mathrm{s}} = \boldsymbol{S}_t \delta \boldsymbol{e}_{\mathrm{s}}, \tag{13}$$

$$\delta \boldsymbol{d}_{\mathrm{s}} = \boldsymbol{S}_d \delta \boldsymbol{e}_{\mathrm{s}}, \tag{14}$$

where $\boldsymbol{S}_d = \boldsymbol{B}^{+}\left[\boldsymbol{I} - \boldsymbol{F}\boldsymbol{V}_{\mathrm{s}}(\boldsymbol{V}_{\mathrm{s}}^{\mathrm{T}}\boldsymbol{F}\boldsymbol{V}_{\mathrm{s}})^{-1}\boldsymbol{V}_{\mathrm{s}}^{\mathrm{T}}\right]$ and $\boldsymbol{S}_t = -\boldsymbol{V}_{\mathrm{s}}(\boldsymbol{V}_{\mathrm{s}}^{\mathrm{T}}\boldsymbol{F}\boldsymbol{V}_{\mathrm{s}})^{-1}\boldsymbol{V}_{\mathrm{s}}^{\mathrm{T}}$.

The target of the active control is to acquire the control amount for the selected structural elements. The targets of the internal force for force control and the nodal displacement vector for shape control are set to $\boldsymbol{t}^*$ and $\boldsymbol{d}^*$, respectively. Then, the required increments to accomplish the goals are

$$\delta \boldsymbol{t}_{\mathrm{s}} = \boldsymbol{t}^* - \boldsymbol{t}, \tag{15}$$

$$\delta \boldsymbol{d}_{\mathrm{s}} = \boldsymbol{d}^* - \boldsymbol{d}. \tag{16}$$

Considering that the basic calculation processes for force and shape control are similar, Eq. (17) is applied for the unified expression to substitute for Eqs. (13) and (14). Similarly, Eq. (18) is used to substitute for Eqs. (15) and (16) in the following:

$$\delta \boldsymbol{x}_{\mathrm{s}} = \boldsymbol{S}_x \delta \boldsymbol{e}_{\mathrm{s}}, \tag{17}$$

$$\delta \boldsymbol{x}_{\mathrm{s}} = \boldsymbol{x}^* - \boldsymbol{x}. \tag{18}$$

The mathematical model for the active control can be illustrated as

$$\text{Find } \delta \boldsymbol{e}_{\mathrm{s}} = \left\{\delta e_{\mathrm{s}}^1, \delta e_{\mathrm{s}}^2, \delta e_{\mathrm{s}}^3, \ldots, \delta e_{\mathrm{s}}^{n_{\mathrm{a}}}\right\}, \tag{19}$$

$$\text{s.t. } \boldsymbol{x} = \boldsymbol{x}^*,\ \boldsymbol{A}\boldsymbol{t} = \boldsymbol{f},$$

where n_{a} is the number of active members. To find the control amount for the active members, $\delta \boldsymbol{e}_{\mathrm{s}}$ should be divided into $\delta \boldsymbol{e}_{\mathrm{s}}^{\mathrm{c}}$ for active members and $\delta \boldsymbol{e}_{\mathrm{s}}^{\mathrm{u}}$ for non-active members. Correspondingly, $\delta \boldsymbol{x}_{\mathrm{s}}$ can be separated into two parts: degrees of freedom that need to be controlled $\delta \boldsymbol{x}_{\mathrm{s}}^{\mathrm{c}}$, and degrees of freedom without control $\delta \boldsymbol{x}_{\mathrm{s}}^{\mathrm{u}}$. The number of degrees of freedom that need to be controlled is represented as m_{c}. Correspondingly, the matrix $\boldsymbol{S}_x$ can be split into four parts. Then, Eq. (17) can be rewritten as

$$\begin{Bmatrix}\delta \boldsymbol{x}_{\mathrm{s}}^{\mathrm{c}} \\ \delta \boldsymbol{x}_{\mathrm{s}}^{\mathrm{u}}\end{Bmatrix} = \begin{bmatrix}\boldsymbol{S}_x^{11} & \boldsymbol{S}_x^{12} \\ \boldsymbol{S}_x^{21} & \boldsymbol{S}_x^{22}\end{bmatrix}\begin{Bmatrix}\delta \boldsymbol{e}_{\mathrm{s}}^{\mathrm{c}} \\ \delta \boldsymbol{e}_{\mathrm{s}}^{\mathrm{u}}\end{Bmatrix}. \tag{20}$$

Since the control amount of passive members is zero such that $\delta \boldsymbol{e}_{\mathrm{s}}^{\mathrm{u}} = \boldsymbol{0}$, Eq. (20) can be rearranged as

$$\delta \boldsymbol{x}_{\mathrm{s}}^{\mathrm{c}} = \boldsymbol{S}_x^{11}\delta \boldsymbol{e}_{\mathrm{s}}^{\mathrm{c}}, \tag{21}$$

where the row of $\boldsymbol{S}_x^{11}$ is m_{c} and the column of $\boldsymbol{S}_x^{11}$ is n_{a}.

The control amount for active members can be solved by Eq. (21); the solution is shown in Eq. (22). $\boldsymbol{S}_x^{11+}$ is the Moore-Penrose pseudoinverse of $\boldsymbol{S}_x^{11}$.

$$\delta \boldsymbol{e}_{\mathrm{s}}^{\mathrm{c}} = \boldsymbol{S}_x^{11+}\delta \boldsymbol{x}_{\mathrm{s}}^{\mathrm{c}}. \tag{22}$$

The procedure of obtaining the control amount is as follows:

1. Initialize $\boldsymbol{t}^{(0)} = \boldsymbol{t}_{\mathrm{f}}$, $\boldsymbol{d}^{(0)} = \boldsymbol{d}_{\mathrm{f}}$, $\boldsymbol{e}^{(0)} = \boldsymbol{e}_{\mathrm{f}}$, where $(\,)_{\mathrm{f}}$ denotes the vector at the loaded end. Set $\boldsymbol{e}_{\mathrm{s}}^{\mathrm{c}(0)} = \boldsymbol{0}$ and $k=0$. Obtain the initial difference to control target $\delta \boldsymbol{x}_{\mathrm{s}}^{\mathrm{c}(0)}$.

2. Calculate the equilibrium matrix $\boldsymbol{A}^{(k)}$ and $\boldsymbol{S}_x^{11(k)}$.

3. Solve $\delta \boldsymbol{e}_{\mathrm{s}}^{\mathrm{c}(k)}$ by Eq. (22).

4. Use the Newton-Raphson method to obtain the equilibrium configuration. Refer to Luo and Lu (2006) for the detailed procedure. After obtaining the equilibrium configuration, the internal force, member elongation, nodal displacement, and control amount are updated for the next step. $\boldsymbol{t}^{(k+1)}=\boldsymbol{t}^{(k)}+\delta \boldsymbol{t}_{\mathrm{s}}^{(k)}$; $\boldsymbol{e}^{(k+1)}=\boldsymbol{e}^{(k)}+\delta \boldsymbol{e}_{\mathrm{s}}^{\prime(k)}$; $\boldsymbol{d}^{(k+1)}=\boldsymbol{d}^{(k)}+\delta \boldsymbol{d}_{\mathrm{s}}^{(k)}$; $\boldsymbol{e}_{\mathrm{s}}^{\mathrm{c}(k+1)}=\boldsymbol{e}_{\mathrm{s}}^{\mathrm{c}(k)}+\delta \boldsymbol{e}_{\mathrm{s}}^{\mathrm{c}(k)}$.

5. Determine the new difference to the control target $\delta \boldsymbol{x}_{\mathrm{s}}^{\mathrm{c}(k+1)}$.

6. Complete the iteration if the difference $\delta \boldsymbol{x}_{\mathrm{s}}^{\mathrm{c}(k+1)}$ satisfies the convergence condition. Otherwise, set k=k+1 and loop from steps 2 to 5.

3 Herringbone ribbed cable dome model

A herringbone ribbed cable dome with adjustable cables was designed and fabricated. The entire model comprised the internal cable dome and the exterior lateral support system.

3.1 Configurations of the herringbone ribbed cable dome

The diameter of the model is 10 m. The height from the hinge support to the top of the dome is 1.5 m. The structure consists of 49 struts and 98 cables. All tension members are designed as length adjustable units. The total number of nodes is 74, in which 12 nodes are pin supports. Every node in the model is designed as a hinge joint. The detailed geometry of the structure is shown in Fig. 1. The design model and experimental model are shown in Fig. 2.

3.2 Section parameters and mechanical properties

The geometric parameters of the tension and compression members for the scale experimental model are listed in Table 1. For convenient assembly and the active control procedure of the dome, all cables are designed to have the ability to change their length. Compressed struts are made of stainless steel round tubes. Young's modulus of the struts is E_{s}=206000 N/mm^2, and the yield stress of the struts is 235 MPa. The section parameter of the strand ropes is 1×19, which indicates one strand with 19 wires. Young's modulus of the cables is E_{c}=160000 N/mm^2, and the ultimate tensile stress is 1670 MPa.

3.3 Design of active units

The active units are indispensable for changing the length of elements. The method of changing the lengths of the cables is selected to change the shape of the structure. The experiment in this study adopts thread casing connections in the cables as mechanical adjustment units. The casing connection is embedded in cables with both positive and negative patterns of the screw. The clockwise rotation of the connection causes contraction of the cables. Conversely, the anti-clockwise rotation causes elongation of the cables. The connection is located at the end of the cable. The adjustment of the cable length is achieved using torque wrenches. A detailed view of the active unit is shown in Fig. 3.

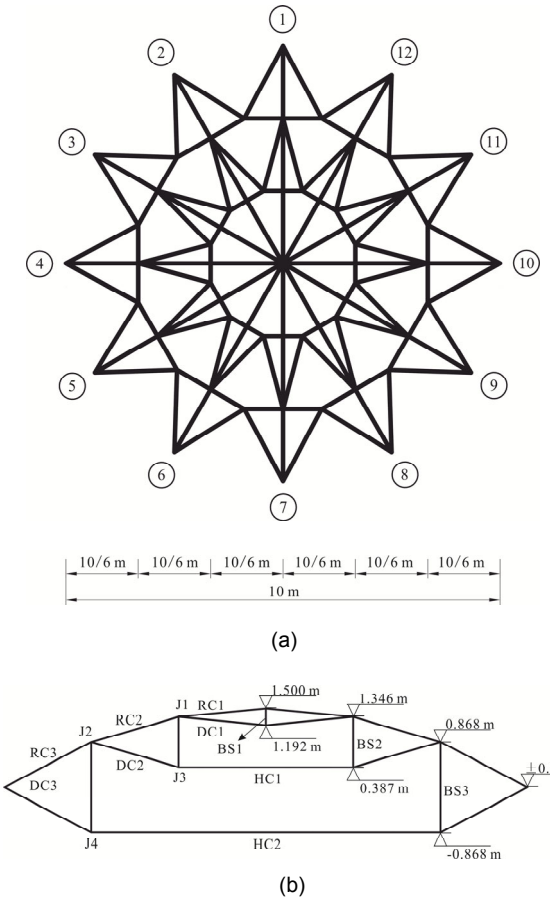

Fig. 1 Cable dome geometry: (a) plan view; (b) section view
RC: ridge cable; DC: diagonal cable; HC: hoop cable; BS: brace strut

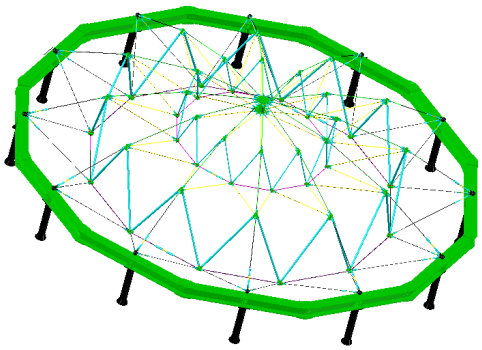

(a)

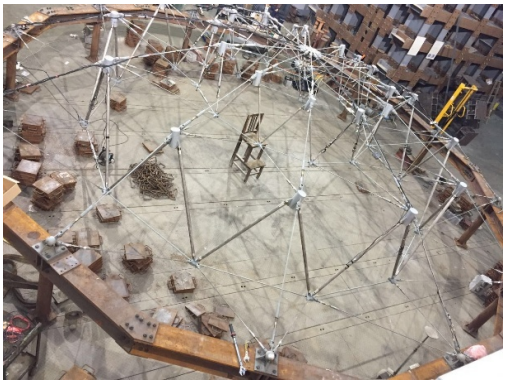

(b)

Fig. 2 Herringbone ribbed cable dome model
(a) Design model; (b) Experimental model

Table 1 Information about cables and struts

Item	Member	Type	Adjustable quantity (mm)
Ridge cable (RC)	RC1	Φ12 mm	50
	RC2	Φ12 mm	50
	RC3	Φ12 mm	50
Diagonal cable (DC)	DC1	Φ10 mm	50
	DC2	Φ10 mm	50
	DC3	Φ10 mm	150
Hoop cable (HC)	HC1	Φ12 mm	50
	HC2	Φ16 mm	50
Brace strut (BS)	BS1	Φ120 mm×5	–
	BS2	Φ25 mm×3	–
	BS3	Φ45 mm×3	–

4 Assembly and pre-stressing experiment

The construction of the cable dome was achieved by assembling members and applying pre-stressing to the dome. The shape-forming process was achieved by pre-stressing the external diagonal cables using torque wrenches. To obtain the relationship between the torque value and the axial force in the cable, the cable must be calibrated first. Twenty-four external diagonal cables were calibrated, and the calibration results are shown in Fig. 4. Twenty-four cables were divided into four groups, six cables in each group. The relationship between the cable force and the torque value was close to linear. The mean value of the axial force at 40 N·m was set to be the initial design value of the external diagonal cables (DC3) for the experiment, which is 13.67 kN.

(a)

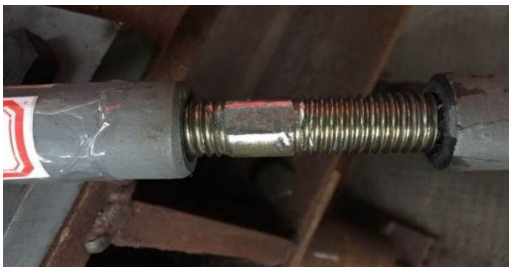

(b)

Fig. 3 Detailed view of the active unit
(a) Diagrammatic sketch; (b) Actual model

To obtain the internal force of the structural members, cable force sensors (Fig. 5a), a cable dynamometer (Fig. 5b), and strain gauges were employed during the test. The displacement of the free nodes was acquired by the Leica TCRA1201+ total station instrument. Considering that the cable dome had large number of elements and the structure was geometrically symmetric, 14 force sensors were arranged in the cables which were located in axis 1 and axis 4, as shown in Fig. 6. The strain gauges were also located in the vertical axis direction for the compression force measurements of the struts, as shown in Fig. 7. To eliminate the bending effect of the struts, two strain gages were mounted on each strut. For the central compression strut, four strain gages were fitted on it. A total of 37 measuring points of the strain gauges including one point for temperature

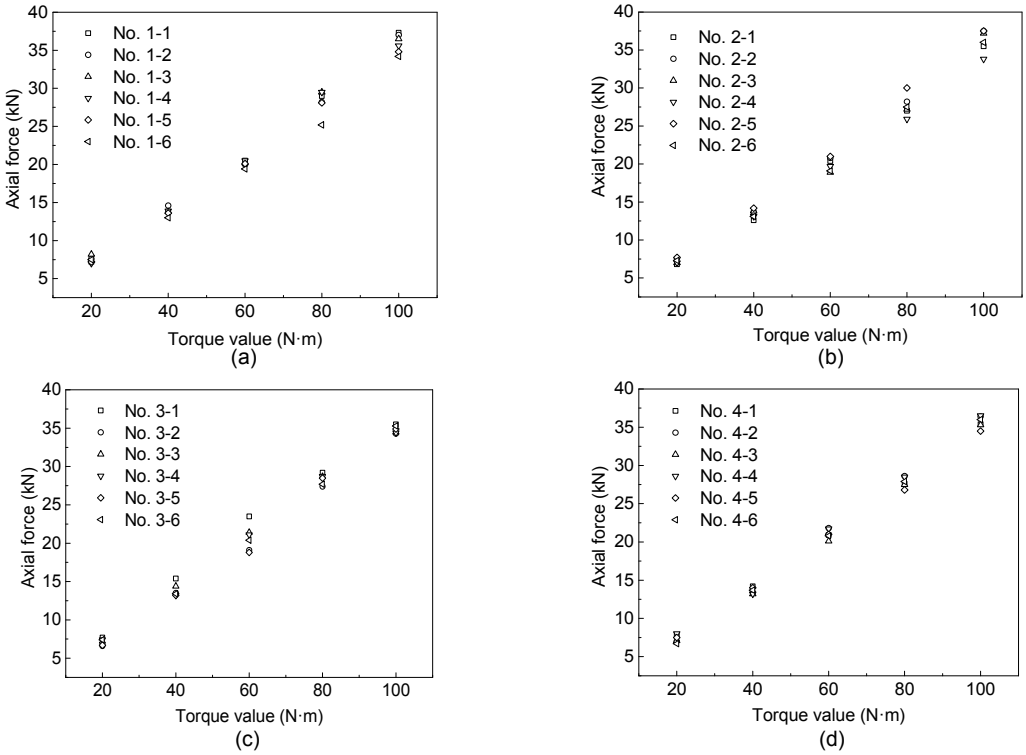

Fig. 4 Relationship between the external diagonal cable force and the torque value
Calibration results of group 1 (a), group 2 (b), group 3 (c), and group 4 (d)

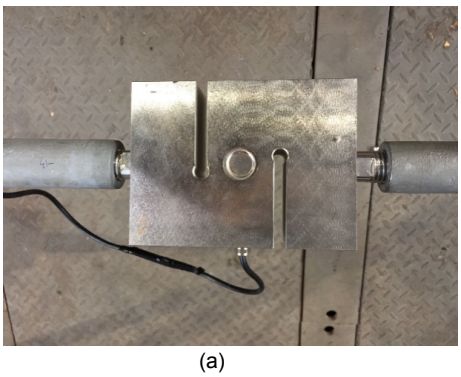

Fig. 5 Force measuring instruments
(a) Cable force sensor; (b) Cable dynamometer

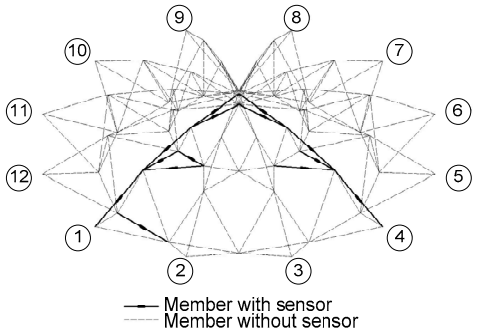

Fig. 6 Layout of the force sensors

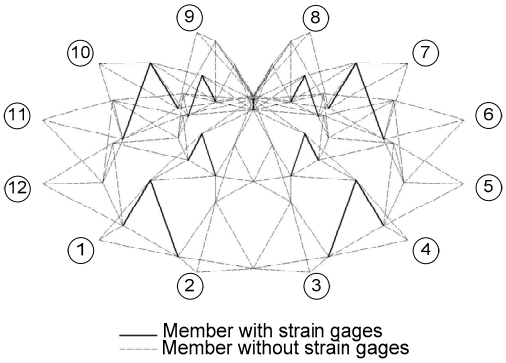

Fig. 7 Layout of the strain gages

compensation were installed for the structure. The position for measuring the nodal displacement was set on the top of every upper joint, as shown in Fig. 8.

The theoretical initial pre-stress in cables and struts can be obtained from the approach of integral feasible pre-stress by the equilibrium matrix theory (Yuan and Dong, 2002). The analysis results indicated that only one integral feasible pre-stress exists for the herringbone ribbed cable dome. Then, the design pre-stress force of the entire structure can be achieved by setting the force of the external diagonal cables to the expected value.

Because a total of 24 cables needed to be adjusted, a reasonable pre-stressing plan was required to ensure that these cables would simultaneously attain the same pre-stress level. The pre-stressing plan in this study was as follows:

1. Set the value of the torque wrenches to 20 N·m. Adjust the external diagonal cables in axis 1 and axis 7 simultaneously with torque wrenches to the corresponding value. Then, adjust the external diagonal cables in axes 2-8, 3-9, 4-10, 5-11, and 6-12 successively (refer to Fig. 9).

2. Set the value of the torque wrenches to 30 N·m. Then, pre-stress the external diagonal cables with the same adjustment sequence.

3. Increase the value of the torque wrenches to 40 N·m and successively adjust all external diagonal cables according to Fig. 9.

4. Use the cable dynamometer to measure the force of all external diagonal cables. Fine tune the length of cables if internal forces have deviated from the design value. As every adjustment created a new redistribution of forces, the measurement and adjustment process was an iterative procedure. The adjustment continued until the pre-stress values of all external diagonal cables were close to the design level.

After the dome was pre-stressed, the comparison of theoretical and experimental pre-stress distribution of the structure was performed, as shown in Table 2. The experimental value I was received from the force sensors and strain gages.

For cables without the arrangement of force sensors, the cable dynamometer was used to obtain the internal force in all cables. The experimental value II is the mean value acquired from the cable dynamometer of each type of cable. The comparison of theoretical and experimental cable internal forces is displayed in Fig. 10. Both the experimental values of I and II are close to the theoretical value. The

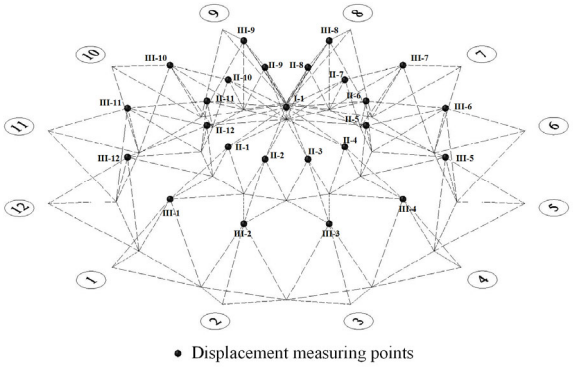

Fig. 8 Layout of the displacement measuring points

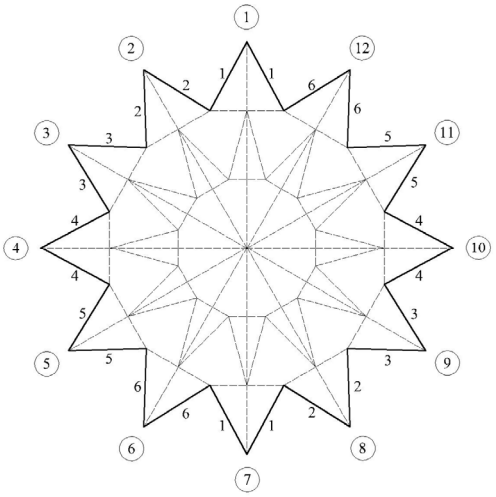

Fig. 9 Adjustment sequence diagram

Table 2 Internal force in structural members of the dome

Member	Theoretical value (kN)	Experimental value I (kN)
RC1	4.839	3.937
RC2	10.329	9.326
RC3	23.276	22.317
DC1	5.130	4.889
DC2	5.764	5.761
DC3	13.667	–*
HC1	19.289	16.588
HC2	37.907	31.280
BS1	−5.524	−5.068
BS2	−1.678	−1.966
BS3	−6.332	−6.233

* No sensors on DC3

deviation of force in HC1 and HC2 is relatively larger than the deviation of force in other cables.

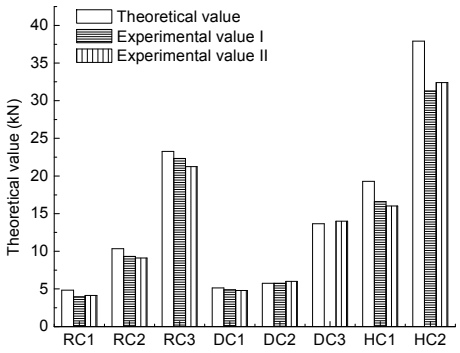

Fig. 10 Comparison of theoretical and experimental cable internal forces

5 Active adjustment test

To obtain the response of the structure when changing the cable lengths, an active adjustment test was conducted to obtain the force variations of elements and the displacements of the nodes. The structure contains eight types of cables: RC1, RC2, RC3, DC1, DC2, DC3, HC1, and HC2. It is desirable to achieve the target with the least number of cables needing to be adjusted. The downward displacements of the structure occur under the action of the vertical load. The contraction of the diagonal cables causes the structure to rise, which enhances its structural performance. Thus, three types of diagonal cables were chosen to implement the active control test.

The ideal adjustment procedure should be a simultaneous changing of the lengths of all cables which were chosen to be adjusted. However, due to the limitation of the experimental conditions, the cables were adjusted successively. The range of length variation [0, −3] mm was set for cable length adjustment, and the adjustment length of each step was −0.5 mm. A minus sign represents contraction of the cables. No load was applied to the structure during the adjustment procedure. Torque wrenches were used to adjust the length of the cables, and the adjustment amount was measured and checked by digital vernier calipers.

The numerical model for the cable dome was established by ANSYS software. Element types LINK 8 and LINK 10 were applied to respectively simulate the struts and cables for the geometrically nonlinear analysis. Twelve external nodes of the structure were set as fixed pin supports.

5.1 Adjustment of DC1

Twelve DC1 from axis 1 to axis 12 were regulated. The internal forces of the cables and the nodal displacements were recorded at the end of each step. The final results are shown in Figs. 11 and 12. The experimental results indicate that the variation trend

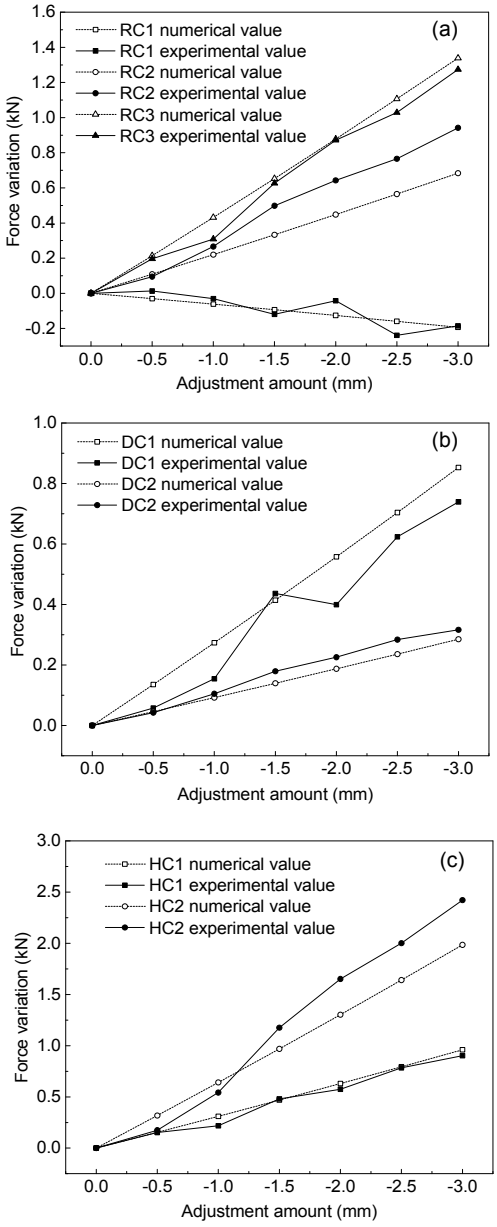

Fig. 11 Internal force variation of the DC1 adjustment
(a) Ridge cables; (b) Diagonal cables; (c) Hoop cables

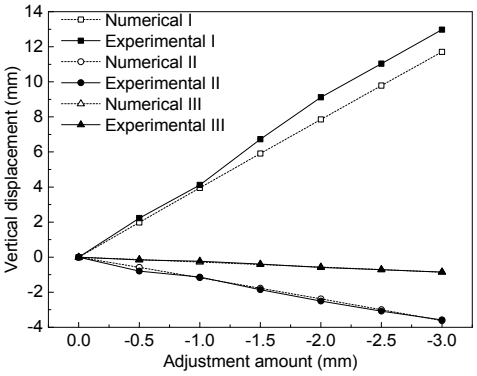

Fig. 12 Vertical displacement of the upper joints of the DC1 adjustment

during the adjustment corresponds with the numerical results. However, some experimental data may differ from the numerical value, and the curve of the test value is not a straight line. The main reason may be an error between the design and the actual coordinates of the nodal joints. Besides, error during the manual adjustment process exists since the adjustment amount in each step is fairly small. The results indicate that the internal force of RC1 decreases, and the nodes of both the inner ring (nodes II) and the external ring (nodes III) have downward displacements.

5.2 Adjustment of DC2

Similarly, the experiment of the adjustment of DC2 was performed after restoring DC1 to its original length. The adjustment amount and sequence for DC2 were similar to the adjustment of DC1. The test results are provided in Figs. 13 and 14. Most of the experimental results correspond with the numerical results, especially for the vertical displacement value. The results show that during the process of adjusting DC2, the internal forces of all cables increase, and the joints of the external ring have downward displacements.

5.3 Adjustment of DC3

The DC3 adjustment experiment was conducted after DC2 was adjusted to its original length. The experimental results are shown in Figs. 15 and 16.

In the process of adjusting DC3, the internal forces of all cables increased. All upper nodes of the dome had upward displacements, and the vertical displacement increments were very similar.

Tables 3 and 4 illustrate the influence of different adjustment plans on the structure. The DC1 adjustment caused decrease of the internal force of RC1 and the displacements of nodes II and III. The DC2 adjustment also caused displacement decline of nodes III. For the DC3 adjustment, both the internal force in the cable members and the displacement of the upper joints increased, which was favorable for improving the total structural performance.

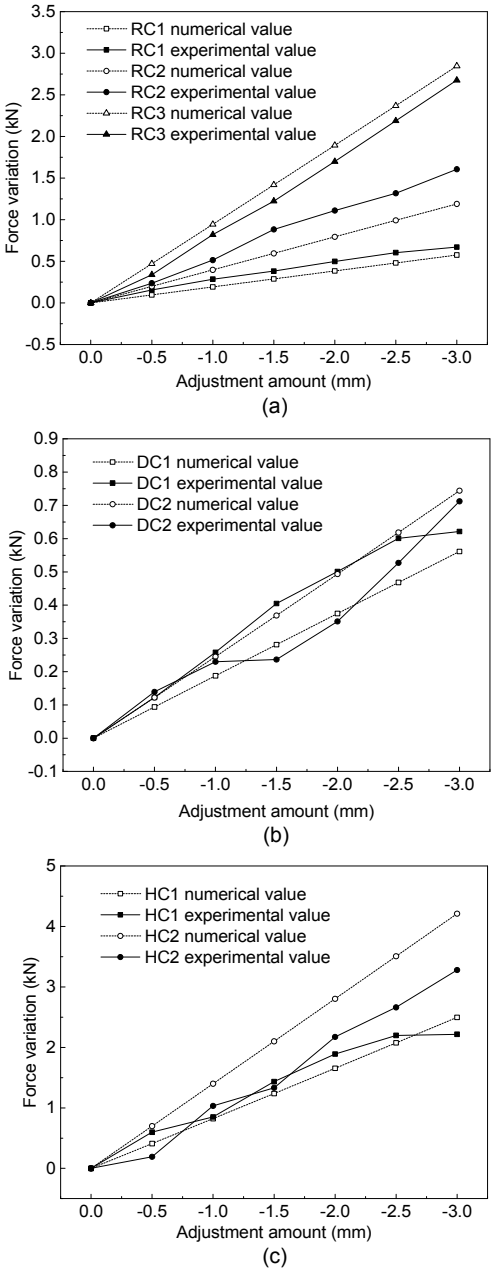

Fig. 13 Internal force variation of the DC2 adjustment
(a) Ridge cables; (b) Diagonal cables; (c) Hoop cables

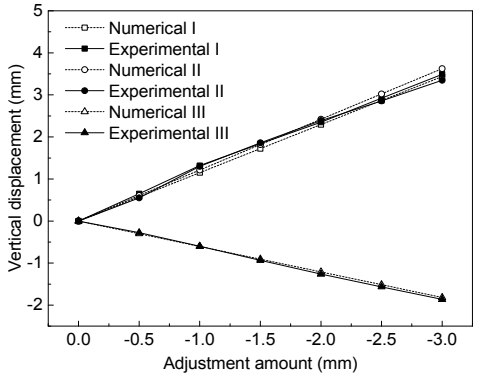

Fig. 14 Vertical displacement of the upper joints of the DC2 adjustment

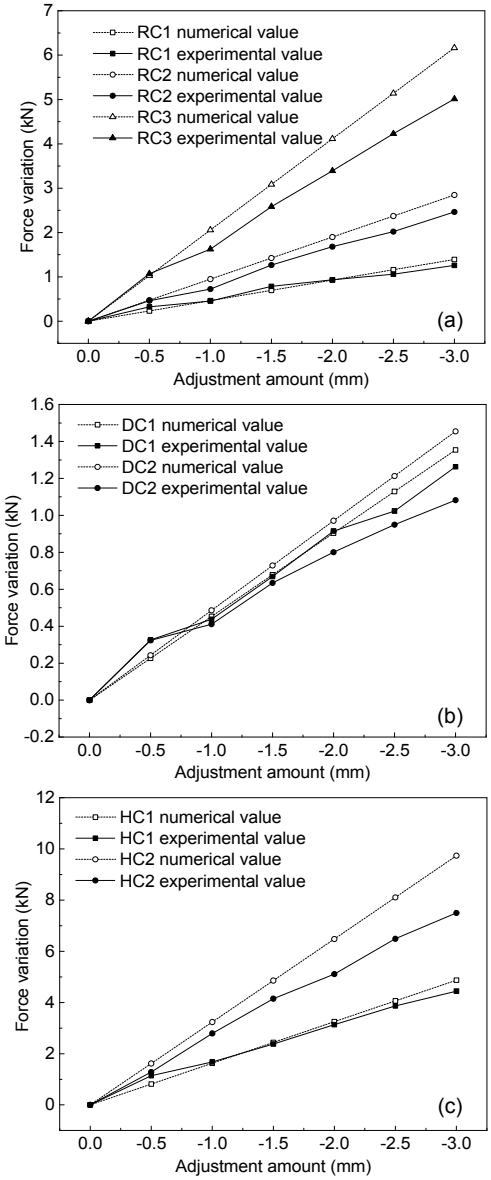

Fig. 15 Internal force variation of the DC3 adjustment
(a) Ridge cables; (b) Diagonal cables; (c) Hoop cables

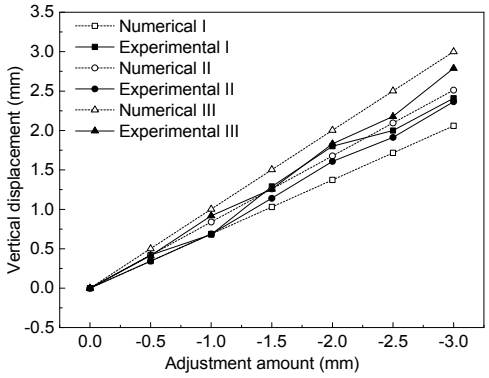

Fig. 16 Vertical displacement of the upper joints of the DC3 adjustment

Table 3 Influence of adjustment to cable internal force

Member type	DC1 adjustment	DC2 adjustment	DC3 adjustment
RC1	↓	↑	↑
RC2	↑	↑	↑
RC3	↑	↑	↑
DC1	↑	↑	↑
DC2	↑	↑	↑
DC3	↑	↑	↑
HC1	↑	↑	↑
HC2	↑	↑	↑

↑: increase; ↓: decrease

Table 4 Influence of adjustment to nodal displacement

Node type	DC1 adjustment	DC2 adjustment	DC3 adjustment
I	↑	↑	↑
II	↓	↑	↑
III	↓	↓	↑

↑: increase; ↓: decrease

It can be concluded that the response of the structure to the DC3 adjustment is greater than that of the structure to the DC1 and DC2 adjustments by the comparison of the internal force variation. If the relaxation of the cables is the failure criterion of the cable domes, the DC3 adjustment is able to obtain a greater internal force increment and is more efficient in preventing failure of the structure. Changing the cable lengths of DC3 is chosen as the way to implement force control and nodal displacement control in the following section.

6 Active control test under static load

In this section, an active control experiment was performed by adjusting the length of DC3. The aim of

the test was to verify the effectiveness of the active control algorithm and to prove the adaptation of the cable dome configuration to different load cases. The performance of the structure can be improved via the control procedure. The control experiment includes two control subjects: the internal force of the selected cables and the displacement of the selected nodes.

As the traditional failure of the structure often begins in the central zone of the cable domes, two control targets are set for the experiment to prevent the slackening of the ridge cables and significant displacements in the central region. The targets are as follows:

1. The top central node (I-1) is restored to a specified position;

2. The inner ridge cables (RC1) will maintain the internal force to a specified level.

Steel blocks were chosen as the static load for the loading test. The weight of each steel block was 20 kg. The blocks were hung on the upper joints of the structure through the wire ropes. The loads were evenly distributed on every upper joint. The layout of the loading point distribution is shown in Fig. 17. A total of 25 loading points was employed. A scheme for the loading process involving five steps was constructed for the test and the loading of each step was 20 kg.

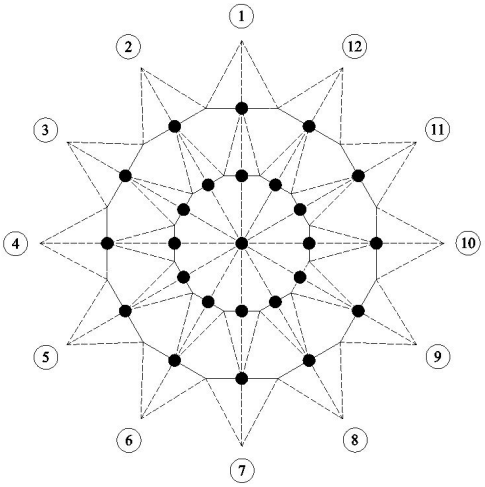

Fig. 17 Loading points layout

Two load cases were set for the active control test. The first load case was the service load case, and the second load case was the excessive load case. The target was to maintain the position of the top central node and the force level of RC1 in the service load case when the structure was under the excessive load case. The detailed procedures are as follows:

1. The cable dome was adjusted to the initial configuration.

2. The weights of 60 kg were applied on every upper joint of the dome to simulate load case 1. Load case 1 was used to simulate the service load case.

3. The weights of 100 kg were applied on every upper joint of the dome to simulate load case 2. Load case 2 was used to simulate the excessive load case.

4. The response of the structure under load case 1 was set as the control target for the dome under load case 2. The length of DC3 was adjusted according to the value obtained from the theoretical calculations to achieve the control objective.

5. The response data of the structure were collected and compared with the theoretical value.

Twenty-four DC3 were selected as the active members to conduct the active control test. To satisfy the two targets, −1.53 mm for target 1 and −1.68 mm for target 2 were achieved by the theory of the active control algorithm in Section 2. Nine steps were designed for the control experiment procedure, as shown in Table 5.

Table 5 Active control test procedure

Procedure	Load (kg)	Adjustment amount (mm)
Initial	0	0
Step 1	60	0
Step 2	100	0
Step 3	100	−0.50
Step 4	100	−1.00
Step 5	100	−1.53
Step 6	100	−1.68
Step 7	100	−2.00
Step 8	100	−2.50
Step 9	100	−3.00

The internal force variation of the cables and the nodal displacements of the free nodes during the control process are shown in Figs. 18 and 19, respectively.

The results indicated that the response of the structure during the control adjustment was generally consistent with the results of the numerical analysis. Only a slight fluctuation of the curve emerged from step 3 to step 9. The general trend of the structural

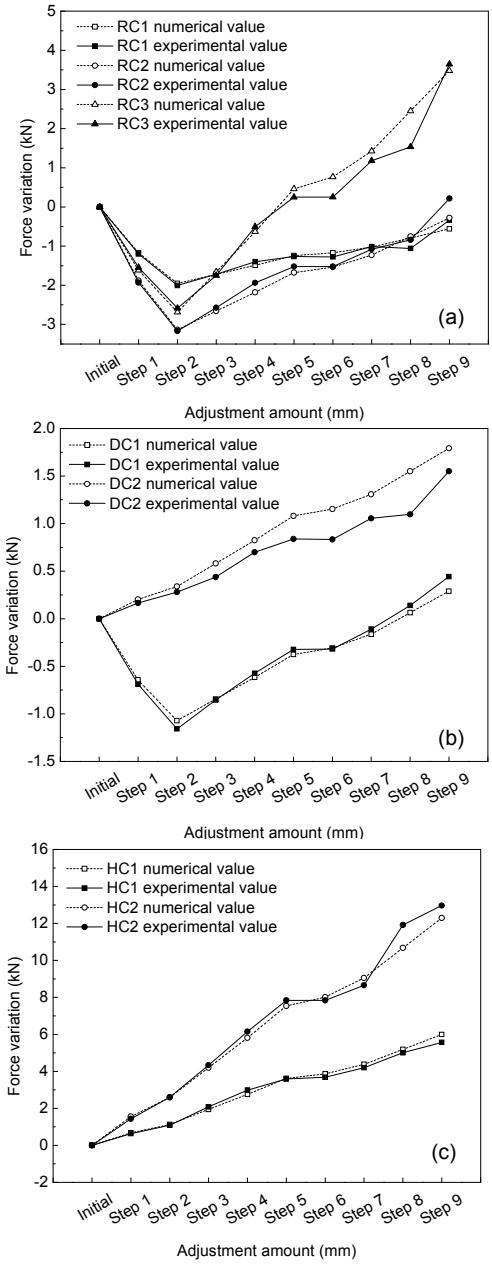

Fig. 18 Internal force variation of the active control experiment: (a) ridge cables; (b) diagonal cables; (c) hoop cables

response was as expected. The evaluation of the active control process is shown in Table 6. The efficiencies of the force control and the shape control were 90.6% and 120.2%, respectively. The experimental results are close to the target value of the theoretical answers. The active control experiment demonstrated the feasibility of the proposed control method.

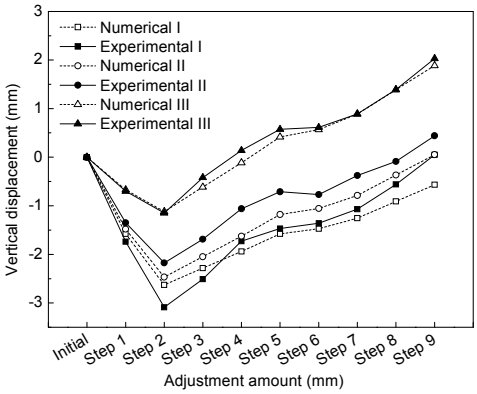

Fig. 19 Vertical displacement of the upper joints of the active control experiment

Table 6 Active control process evaluation

Control target	Internal force of RC1 (kN)	Vertical displacement of the central node (mm)
Load case 1	−1.201	−1.742
Load case 2	−2.007	−3.090
After active control	−1.277	−1.470
Efficiency	90.60%	120.20%

Generally, the force variation and nodal displacement variation tendencies of the experimental results are consistent with the theoretical analysis; however, some differences in the specific data are observed between the measured results and the numerical results. Errors during the active control test can be summarised as follows:

1. Assembly error. Due to the large number of members and nodes of the model, cable-length deviations and node position errors exist during the test. Thus, the different initial configurations of the structure are different from the theoretical model.

2. Numerical model error. The numerical model assumes the cables as linear elements and the free nodes as ideal hinge joints. However, the actual cables are composed of two parts: the active control unit and the steel strand. The elastic modulus and the section properties of the cables may have different parameters with respect to the theoretical calculations.

3. Manual adjustment error. Due to errors in the artificial adjustment during the control procedure, the actual value of the adjustment amount may slightly differ from the expected value.

7 Conclusions

The active control experiment on a new form of cable dome, the herringbone ribbed cable dome, is presented in this study.

An algorithm based on the nonlinear force method is proposed for the active control of a herringbone ribbed cable dome. The calculation can obtain the control amount for the specified control objectives, such as maintaining the force level of the members and controlling the displacements of the free nodes. The method can be also used in different types of cable domes, for instance, the Geiger type and the Levy type and even tensegrity structures.

By adjusting the lengths of the external diagonal cables using torque wrenches, the theoretical prestressing level of the dome can be attained. Based on the active adjustment test of three different types of diagonal cables, the adjustment of the cables in the external ring is more reasonable and effective for enhancing the total structural performance than the adjustment of the cables in the inner or middle rings.

The active control experiment verifies that adjusting the lengths of the cables can change the selected member force and the nodal displacement. A more reasonable stress state can be achieved by changing the member length of the structure. The active control method is able to increase the capability of the structure to withstand excessive loads. Since the cable dome structure is highly sensitive to the lengths of the cables, the accuracy of control relies on the precise control of a number of cables. High-precision actuators are required to enable the practical application of an adaptive cable dome. This paper focuses on active control by using symmetrically arranged actuators, and further research could be concentrated on adding a more complex case to active control where symmetry is abandoned for different kinds of cable domes.

References

Adam B, Smith IF, 2007. Self-diagnosis and self-repair of an active tensegrity structure. *Journal of Structural Engineering*, 133(12):1752-1761. https://doi.org/10.1061/(ASCE)0733-9445(2007)133:12(1752)

Adam B, Smith IFC, 2008. Active tensegrity: a control framework for an adaptive civil-engineering structure. *Computers & Structures*, 86(23-24):2215-2223. https://doi.org/10.1016/j.compstruc.2008.05.006

Chen LM, Dong SL, 2011. Dynamical characteristics research on cable dome. *Advanced Materials Research*, 163-167:3882-3886. https://doi.org/10.4028/www.scientific.net/AMR.163-167.3882

Djouadi S, Motro R, Pons JC, et al., 1998. Active control of tensegrity systems. *Journal of Aerospace Engineering*, 11(2):37-44. https://doi.org/10.1061/(ASCE)0893-1321(1998)11:2(37)

Dong SL, Liang HQ, 2014. Mechanical characteristics and analysis of prestressing force distribution of herringbone ribbed cable dome. *Journal of Building Structures*, 35(6):102-108 (in Chinese). https://doi.org/10.14006/j.jzjgxb.2014.06.012

Fest E, Shea K, Domer B, et al., 2003. Adjustable tensegrity structures. *Journal of Structural Engineering*, 129(4):515-526. https://doi.org/10.1061/(ASCE)0733-9445(2003)129:4(515)

Fest E, Shea K, Smith IFC, 2004. Active tensegrity structure. *Journal of Structural Engineering*, 130(10):1454-1465. https://doi.org/10.1061/(ASCE)0733-9445(2004)130:10(1454)

Fuller RB, 1962. Tensile-integrity Structures. US Patent 3063521.

Geiger DH, Stenfaniuk A, Chen D, 1986. The design and construction of two cable domes for the Korean Olympics. Proceedings of the IASS Symposium on Shells, Membranes and Space Frames, p.265-272.

Guo JM, Zhu ML, 2016. Negative Gaussian curvature cable dome and its feasible prestress design. *Journal of Aerospace Engineering*, 29(3):04015077. https://doi.org/10.1061/(ASCE)AS.1943-5525.0000585

Kim SD, Sin IA, 2014. A comparative analysis of dynamic instability characteristic of Geiger-typed cable dome structures by load condition. *Journal of the Korean Association for Spatial Structures*, 14(1):85-91. https://doi.org/10.9712/KASS.2014.14.1.085

Kmet S, Mojdis M, 2015. Adaptive cable dome. *Journal of Structural Engineering*, 141(9):04014225. https://doi.org/10.1061/(ASCE)ST.1943-541X.0001189

Korkmaz S, Ali NBH, Smith IFC, 2012. Configuration of control system for damage tolerance of a tensegrity bridge. *Advanced Engineering Informatics*, 26(1):145-155. https://doi.org/10.1016/j.aei.2011.10.002

Levy MP, 1994. The Georgia dome and beyond: achieving lightweight-longspan structures. Spatial, Lattice and Tension Structures: Proceedings of the IASS-ASCE International Symposium, p.560-562.

Li KN, Huang DH, 2011. Static behavior of Kiewitt6 suspendome. *Structural Engineering and Mechanics*, 37(3):309-320. https://doi.org/10.12989/sem.2011.37.3.309

Luo YZ, Lu JY, 2006. Geometrically non-linear force method for assemblies with infinitesimal mechanisms. *Computers & Structures*, 84(31-32):2194-2199. https://doi.org/10.1016/j.compstruc.2006.08.063

Oppenheim IJ, Williams WO, 1997. Tensegrity prisms as adaptive structures. Proceedings of the ASME International Mechanical Engineering Congress and Exposition, p.113-120.

Pellegrino S, 1990. Analysis of prestressed mechanisms. *International Journal of Solids and Structures*, 26(12): 1329-1350. https://doi.org/10.1016/0020-7683(90)90082-7

Pellegrino S, Calladine CR, 1986. Matrix analysis of statically and kinematically indeterminate frameworks. *International Journal of Solids and Structures*, 22(4):409-428. https://doi.org/10.1016/0020-7683(86)90014-4

Pellegrino S, Kwan ASK, van Heerden TF, 1992. Reduction of equilibrium, compatibility and flexibility matrices, in the force method. *International Journal for Numerical Methods in Engineering*, 35(6):1219-1236. https://doi.org/10.1002/nme.1620350605

Skelton RE, de Oliveira MC, 2009. Tensegrity Systems. Springer, Boston, MA, USA.

Soong TT, Manolis GD, 1987. Active structures. *Journal of Structural Engineering*, 113(11):2290-2302. https://doi.org/10.1061/(ASCE)0733-9445(1987)113:11(2290)

Tang JM, Shen ZY, 1998. The analysis of static mechanical properties for cable domes. *Spatial Structures*, 4(3):17-25. https://doi.org/10.13849/j.issn.1006-6578.1998.03.003

van de Wijdeven J, de Jager B, 2005. Shape change of tensegrity structures: design and control. American Control Conference, p.2522-2527. https://doi.org/10.1109/ACC.2005.1470346

Wang ZH, Yuan XF, Dong SL, 2010. Simple approach for force finding analysis of circular Geiger domes with consideration of self-weight. *Journal of Constructional Steel Research*, 66(2):317-322. https://doi.org/10.1016/j.jcsr.2009.09.010

Wei DM, Li D, Liu YQ, 2015. Dominant modals of wind-induced vibration response for spherical Kiewitt cable dome. *Advanced Materials Research*, 1065-1069: 1156-1159. https://doi.org/10.4028/www.scientific.net/AMR.1065-1069.1156

Xi Y, Xi Z, Qin WH, 2011. Form-finding of cable domes by simplified force density method. *Proceedings of the Institution of Civil Engineers-Structures and Buildings*, 164(3):181-195. https://doi.org/10.1680/stbu.9.00066

Xu X, Luo Y, 2009. Non-linear displacement control of prestressed cable structures. *Proceedings of the Institution of Mechanical Engineers, Part G: Journal of Aerospace Engineering*, 223(7):1001-1007. https://doi.org/10.1243/09544100JAERO455

You Z, 1997. Displacement control of prestressed structures. *Computer Methods in Applied Mechanics and Engineering*, 144(1-2):51-59. https://doi.org/10.1016/S0045-7825(96)01164-4

Yuan XF, Dong SU, 2002. Nonlinear analysis and optimum design of cable domes. *Engineering Structures*, 24(7): 965-977. https://doi.org/10.1016/S0141-0296(02)00017-2

Zhang LM, Chen WJ, Dong SL, 2014. Natural vibration and wind-induced response analysis of the non-fully symmetric Geiger cable dome. *Journal of Vibroengineering*, 16(1):31-41.

Zhu ML, Dong SL, Yuan XF, 2013. Failure analysis of a cable dome due to cable slack or rupture. *Advances in Structural Engineering*, 16(2):259-271. https://doi.org/10.1260/1369-4332.16.2.259

中文概要

题　目： 肋环人字型索穹顶主动控制试验研究

目　的： 本文选取一大型肋环人字型索穹顶结构模型为试验对象进行主动控制试验研究，验证主动控制方法应用于索杆张力结构的可行性。

创新点： 1. 提出通过改变索杆张力结构的形状来提高结构承载性能的方法，并基于非线性力法提出索杆张力结构形状控制和内力控制的计算模型。2. 设计具有长度可调拉索单元的肋环人字型索穹顶模型进行主动控制试验研究，并将结构响应的试验结果与理论计算结果进行对比。

方　法： 1. 以结构形状和杆件内力为控制目标建立求解主动单元调控量的计算模型，编制计算程序进行主动单元调控量的计算；2. 通过对具有拉索长度可调单元的肋环人字型索穹顶进行模型试验研究，考察结构主动调控过程和主动控制过程的结构响应情况。

结　论： 1. 基于非线性力法推导索杆张力结构的结构响应计算公式，推导结果可应用于结构主动控制的计算中；2. 对具有拉索长度可调单元的肋环人字型索穹顶进行模型试验研究，结果表明利用本文提出的理论方法得到的控制方案可达到所设定的结构控制目；3. 试验值与理论计算值数据吻合良好，验证本文理论计算模型的正确性和应用于实际结构的可行性。

关键词： 肋环人字型索穹顶结构；主动控制；非线性力法；内力控制；形状控制